

Tailoring the ferromagnetic surface potential landscape by a templating two-dimensional metal-organic porous network

Lu Lyu^{†,*}, Martin Anstett[†], Ka Man Yu[†], Azadeh Kadkhodazadeh[†], Martin Aeschlimann[†], Benjamin Stadtmüller^{†,§,*}

¹Department of Physics and Research Center OPTIMAS, Rheinland-Pfälzische Technische Universität Kaiserslautern-Landau, Erwin-Schrödinger-Straße 46, 67663 Kaiserslautern, Germany.

²Institute of Physics, Johannes Gutenberg University Mainz, Staudingerweg 7, 55128 Mainz, Germany.

*Email: llyu@rhrk.uni-kl.de

*Email: bstadtmueller@physik.uni-kl.de

Abstract

Two-dimensional metal-organic porous networks (2D-MOPNs) have been identified as versatile nanoarchitectures to tailor surface electronic and magnetic properties on noble metals. In this context, we propose a protocol to redecorate a ferromagnetic surface potential landscape using a 2D-MOPN. Ultrathin cobalt (Co) films grown on Au(111) exhibit a well-ordered surface triangular reconstruction. On the ferromagnetic surface, the adsorbed 2,4,6-tris(4-pyridyl)-1,3,5-triazine (T4PT) molecules can coordinate with the native Co atoms to form a large-scale Co-T4PT porous network. The Co-T4PT network with periodic nanocavities serves as a templating layer to reshape the ferromagnetic surface potential. The subsequently deposited C₆₀ molecules are steered by the network porous potential and the neighboring C₆₀ interactions. The prototype of the ferromagnetic-supported 2D-MOPN is a promising template for the tailoring of molecular electronic and spin properties.

Introduction

Two-dimensional metal-organic porous networks (2D-MOPNs) have been sought-after nanoarchitectures for exotic tessellation patterns¹, catalytic reactions², magnetic exchange^{3,4} and surface quantum confinements⁵. The protocol for fabricating a low-dimensional metal-organic architecture is based on the surface self-assembly between organic molecules and metal adatoms⁶. The selected molecule with an electronegative ligand in the end-group activates a robust coordination with the surface metal adatoms. Such a directional metal-ligand interaction can trigger the formation of a long-range ordered porous nanoarchitecture. To enhance surface self-assembly, 2D-MOPNs are typically fabricated on weakly interacting substrates such as low-index noble metals⁶ and 2D materials⁷. Each organic molecule on the substrates can form an effective potential barrier that blocks the penetration of surface electrons and atoms⁵, analogously to the adatom-induced scattering⁸. Therefore, the periodic nanocavities in a 2D-MOPN are a quantum well array, in which the porous potential can capture the electrons⁹, adatoms¹⁰ and even molecules¹¹. The self-assembly of a 2D-MOPN alters the surface potential landscape of the substrate, thus dictating the arrangement of subsequent adsorbates.

The organic/ferromagnetic interface plays an essential role in molecular spintronics¹², but intense surface activity localizes and even dissociates adsorbed molecules¹³. Experimentally, 2D buffer layers such as graphene¹⁴ and h-BN¹⁵ are applied to passivate and redecorate the ferromagnetic surfaces. The exploration of a 2D robust nanoporous architecture as a decoupling and templating layer for the tailoring of a ferromagnetic surface potential landscape remains uncharted.

In this article, we propose a protocol for self-assembling a 2D-MOPN on an ultrathin ferromagnetic film. On an ultrathin Co film (5 monolayers (ML)), the deposited 2,4,6-tris(4-pyridyl)-1,3,5-triazine (T4PT) molecules can coordinate surface Co atoms to form an ordered Co-T4PT porous network. The large-scale porous architecture reshapes the Co surface potential, thus tailoring the arrangement of the subsequently adsorbed C₆₀ molecules.

Results and Discussions

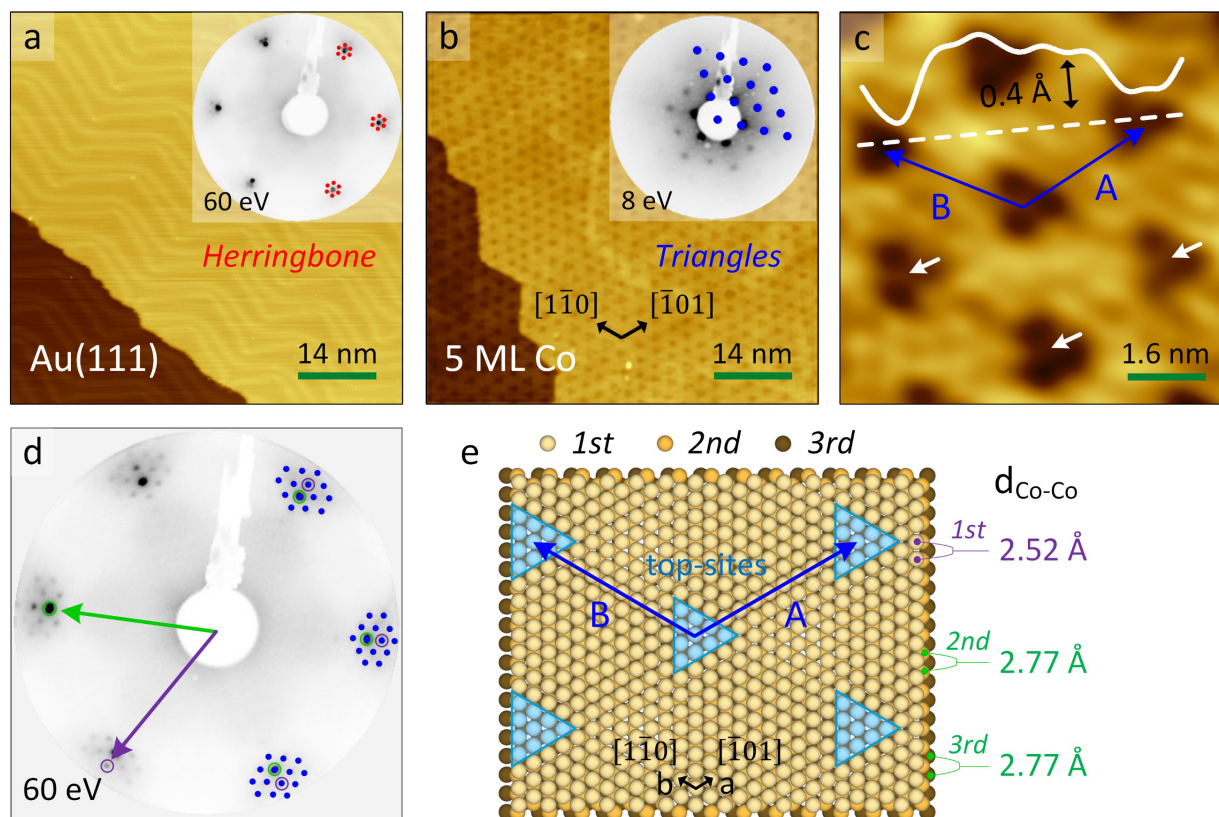


Figure 1. (a) STM topography of Au(111), showing the surface herringbone reconstruction. The corresponding LEED structure (at 60 eV) is overlapped by the herringbone lattice of $(22 \times \sqrt{3})$ (red dots in the right part). (b) STM topography of 5 monolayers (ML) Co on Au(111) shows a triangular surface reconstruction. The LEED image at 8 eV indicates the reconstructed lattice of (11×11) , overlapped by the blue dots in the right corner. (c) High-resolved STM resolves triangular structures with a lattice of $|\mathbf{A}| = |\mathbf{B}| = 28 \pm 2 \text{ \AA}$ and an average depth of 0.4 Å in the line profile. The white arrows indicate clusters in the triangles. (d) LEED image of the 5 ML Co at 60 eV shows multiple diffraction spots from the triangular reconstruction (blue dots), first layer (1st) Co lattice (purple circles) and underneath layers Co lattice (green circles). (e) The proposed model of the top three layers of the Co. The labeled Co lattice ($d_{\text{Co-Co}}$) is 2.52 Å in 1st layer and 2.77 Å in the second (2nd) and third (3rd) layers. The blue triangular regions mark the Co atoms with top-sites stacking in the layers, and they form a periodic pattern with the vectors of \mathbf{A} and \mathbf{B} corresponding to the triangular lattice in (c). All STM images were recorded at 297 K, and the tip bias (V_{tip}) was + 1.02 V in (a) and + 0.79 V in (b, c).

The cleaned Au(111) surface in Figure 1a shows the well-ordered herringbone reconstruction¹⁶, in which the bright waves are generated by the surface stacking faults of face-centered cubic (FCC) and hexagonal close-packed (HCP). The corresponding LEED image indicates the diffraction structures (red dots) of the reconstructed lattice of the $(22 \times \sqrt{3})$. After further deposition of 5

monolayers (ML) Co on the Au surface, the grown films are annealed at 560 K to create a large-scale surface terrace. As shown in [Figure 1b](#), the post-annealed Co surface forms the massive triangular reconstructions, and the LEED image at 8 eV exhibits the first-order diffraction spots of the periodic triangles. The highly resolved STM topography in [Figure 1c](#) resolves the reconstructed units with a lattice of $|\mathbf{A}| = |\mathbf{B}| = 28 \pm 2 \text{ \AA}$ along the surface $\langle 1\bar{1}0 \rangle$ directions, and the line profile across the dark triangles shows an average depth of 0.4 \AA . These indicate the triangular reconstruction resulting from a lattice mismatch of the surface Co layers. It is well known that the lattice of a Co(0001) crystal (2.50 \AA) is very different from that of an Au(111) surface (2.88 \AA), and the post-annealed Co films on Au(111) can form a pseudomorphic growth (lattice-matched epitaxy) in the first few layers^{17,18}. The annealing temperature ($< 575 \text{ K}$) limits the diffusion of the substrate Au atoms in the Co films, but facilitates a surface relaxation of the top Co layer.

In [Figure 1d](#), the LEED image at 60 eV shows multiple diffraction structures, where the highest-intensity spots (green circles) are from a lattice of 2.77 \AA (close to Au(111) surface lattice) and the peripherally adjacent spots (purple circles) are from a lattice of 2.52 \AA (close to Co(0001) crystal lattice). Therefore, a model of the relaxation Co layers is proposed in [Figure 1e](#). The atoms in the top Co layer retain the symmetry (no rotation) but have a smaller lattice of 2.52 \AA than the layers below (2.77 \AA). The lattice mismatch induces a stacking fault between the layers, and the blue triangular regions indicate the top-sites stacking Co atoms forming a superlattice of $(11 \times 11) R0^\circ$. The stacking patterns have a size and a lattice consistent with the triangular reconstruction in [Figure 1c](#), and the reciprocal structures of the $(11 \times 11) R0^\circ$ are well superimposed on the diffraction spots (blue dots) in [Figure 1b](#) and [1d](#).

Furthermore, a reciprocal diffraction simulation is performed on the model of the top three Co layers in [Figure S1](#), and the simulated spots reproduce the intensities and positions of the experimental LEED. However, there are some differences between the triangular structures in [Figure 1c](#) and the typical moiré patterns¹⁹ because some dark triangles vary in size and exhibit a cluster structure in the centers (indicated by white arrows). These characters indicate that the triangles on the Co surface are from the annealing-induced triangular dislocation loops (TDLs)²⁰⁻²². At the top sites, the stacking atoms in the top layer can squeeze out the underlying atoms because of strain relief, creating some atomic vacancies in the second Co layer. Therefore, the generations of TDLs maintain consistency with the stacking regions at the surface top sites.

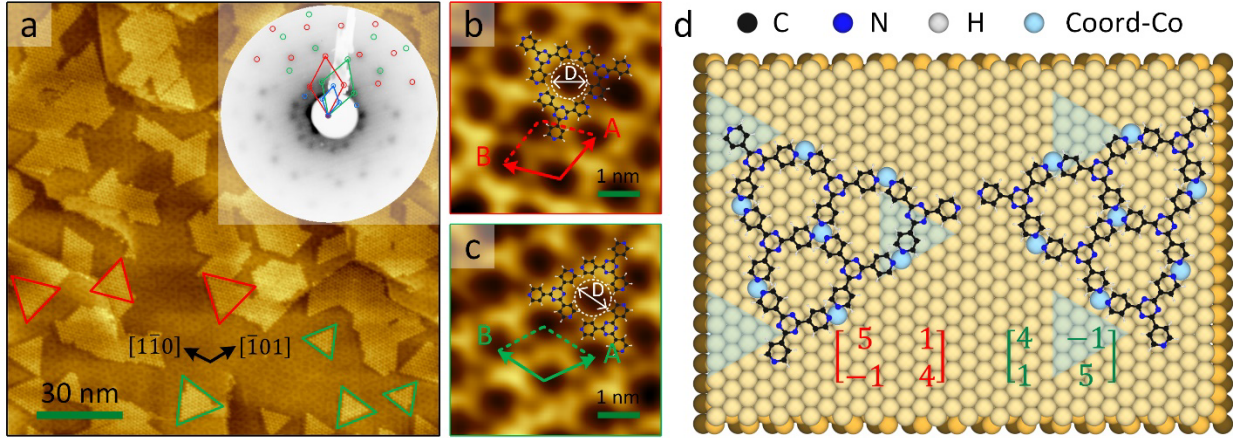


Figure 2. (a) Large-scale STM topography of 0.4 ML Co-T4PT network grown on 5 ML Co surface. The two types of Co-T4PT networks (red and green triangles) are marked corresponding to the mirror diffraction structures (red and green rhombi) in the LEED image (at 18 eV). The blue circles are from the underlying TDL lattice. (b, c) High-resolved STM topographies show the two Co-T4PT porous structures. As shown in the superimposed molecular models, each cavity is composed of three T4PT molecules and has a diameter of $D = 7.5 \pm 0.5 \text{ \AA}$. The mirror superlattices are $\begin{bmatrix} 5 & 1 \\ -1 & 4 \end{bmatrix}$ (red unit cell) and $\begin{bmatrix} 4 & -1 \\ 1 & 5 \end{bmatrix}$ (green unit cell), respectively, corresponding to the overlapping circles in the LEED image. (d) The proposed model of the Co-T4PT mirror networks on the Co surface shows the neighboring T4PT molecules coordinated by a Co adatom (Coord-Co). The blue triangles represent the triangular dislocation loops of the Co surface. All STM were acquired at 106 K, and the V_{tip} was + 0.40 V in (a) and + 0.05 V in (b, c).

On the (111)-terminated coinage metal surfaces (Cu and Au), the adsorbed T4PT molecules with the nitrogen ligands spontaneously coordinate with the surface metal adatoms, self-assembling into 2D-MOPNs²³⁻²⁴. Here, we deposit 0.4 ML T4PT on the 5 ML Co surface, where the as-grown molecules in Figure S2a show some disordered coordinations. A slight annealing at 413 K generates sufficient kinetic energy for molecules and surface Co adatoms (escaping from the TDLs) to fabricate the Co-T4PT porous networks, as depicted in Figure 2a. The LEED image (red and green circles) indicates the mirror structures on the TDL surface, and the red and green triangles in the STM topography identify the two types of triangular networks.

The small-scale STM topographies in Figure 2b and 2c resolve the Co-T4PT mirror lattices: the porous superstructures are described by the matrices of $\begin{bmatrix} 5 & 1 \\ -1 & 4 \end{bmatrix}$ and $\begin{bmatrix} 4 & -1 \\ 1 & 5 \end{bmatrix}$, and the unit cell parameters are $|\mathbf{A}| = |\mathbf{B}| = 11.7 \pm 0.6 \text{ \AA}$ along the $\pm 11^\circ$ to the $\langle 1\bar{1}0 \rangle$ directions. Each cavity is surrounded by three T4PT molecules and the porous size is $D = 7.5 \pm 0.5 \text{ \AA}$, as indicated in the figures. Figure 2d shows the model of the Co-T4PT mirror networks on the Co surface. The neighboring T4PT molecules are coordinated by a Co atom (coord-Co), which is not visible in the STM images as a fragile feature of the single metal-coordinated center²⁵. In the mirror porous

networks, each T4PT molecule is adsorbed at the equivalent position of the Co surface. Due to the intact atomic structure in the top Co layer, the surface TDLs have a negligible effect on the Co-T4PT networks.

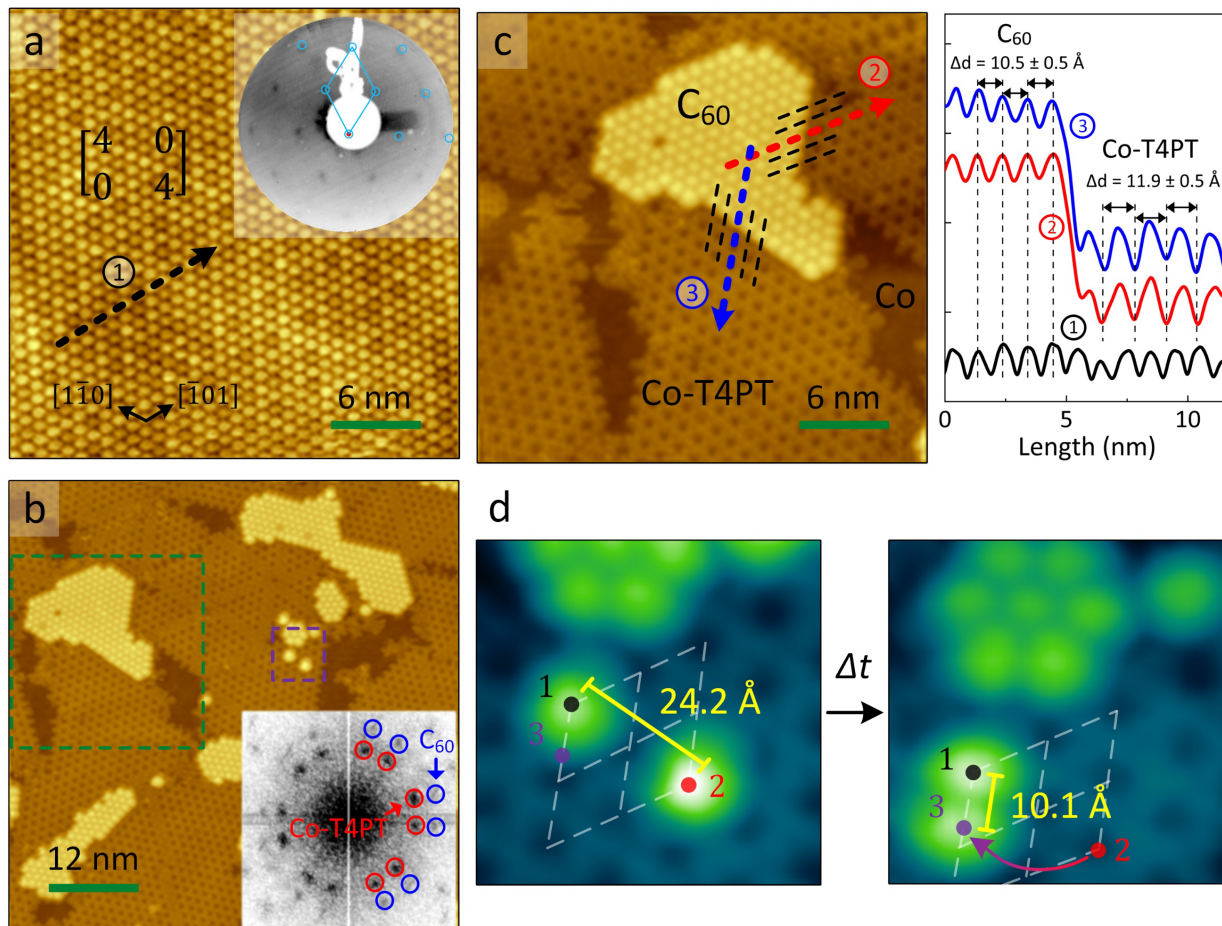


Figure 3. (a) STM topography of 1 ML C₆₀ on 5 ML Co surface. The corresponding LEED image indicates a $(4 \times 4) R0^\circ$ lattice of the C₆₀, overlapped by the light blue circles. (b) STM topography of 0.15 ML C₆₀ on 0.9 ML Co-T4PT network on 5 ML Co surface. The image of the lower-right fast Fourier transform (FFT) ($18 \times 18 \text{ nm}^{-2}$) points out two types of structures from the C₆₀ (out spots marked by the blue circles) and the Co-T4PT (inner spots marked by the red circles) lattices. (c) The zoom-in STM image of the green dashed rectangle in (b). The short-dashed lines indicate the adsorbed C₆₀ molecules following the porous symmetry of the underlying Co-T4PT. In the right part, the line profiles along the color arrows in the structures of (a) and (c). The lattice distances (Δd) of the C₆₀ and the Co-T4PT are $10.5 \pm 0.5 \text{ \AA}$ and $11.9 \pm 0.5 \text{ \AA}$, respectively. (d) Zoom of the purple dashed rectangle in (b). The left and right images are the two real-time STM recorded at a frame interval $\Delta t = 419 \text{ s}$. Left image, two C₆₀ molecules separate at sites "1" and "2" with a distance of 24.2 Å. On the Right image, the two molecules aggregate at the sites "1" and "3" with a distance of 10.1 Å. The white grids show the Co-T4PT porous positions. All STM images were recorded at 106 K, and the V_{tip} was + 0.22 V in (a) and + 0.54 V in (b)-(d).

In a 2D-MOPN, the metal-coordinated organic molecules can create potential barriers to block the penetration of surface electrons, adatoms and even molecules^{5,26}. The well-ordered organic porous architectures form a periodic array of quantum wells through the organic building blocks to trap further adsorbates. For instances, the 2D porous architectures of the BDBA network²⁷ and the NN4A network²⁸ are fabricated on the HOPG surface. Each constructed cavity has a porous size of ~ 8 Å, and the further deposited C₆₀ molecules are trapped in the cavities forming an ordered C₆₀ array. Due to the porous confinement effect, large-scale 2D-MOPN can reshape the entire surface potential landscape. In the following, we explore the behaviors of C₆₀ molecules in the Co-T4PT network on the Co surface.

To understand the surface potential landscape in 5 ML Co, 1 ML C₆₀ molecules are initially deposited on the Co surface, as shown in Figure 3a. The STM topography and the LEED image indicate a commensurate superstructure described by the $(4 \times 4) R0^\circ$, and the lattice is 10.5 ± 0.5 Å along the surface $\langle 1\bar{1}0 \rangle$ directions. In a C₆₀ film, the strong interaction between the molecules²⁹ results in an intermolecular distance equivalent to the C₆₀ van der Waals (vdW) diameter (~ 10 Å)³⁰. Therefore, the C₆₀ molecules adopt a $(4 \times 4) R0^\circ$ configuration on graphene and Cu(111) surfaces^{31,32} with a substrate lattice of ~ 2.5 Å, while they form a $(2\sqrt{3} \times 2\sqrt{3}) R30^\circ$ configuration on Au(111) and Ag(111) surfaces³³ with a substrate lattice of ~ 2.8 Å. In contrast, the (4×4) superlattice on the Co surface reflects that the atomic distance ($d_{\text{Co-Co}}$) in the top Co layer is about 2.5 Å, in agreement with Figure 1e. Furthermore, the STM topography in Figure S3 demonstrates the superlattice matching between the Co surface TDLs (11×11) and the adsorbed C₆₀ molecules (4×4).

In Figure 3b, the Co surface is first covered with a 0.9 ML Co-T4PT porous network, followed by the deposition of 0.15 ML C₆₀ molecules. The C₆₀ molecules tend to aggregate into ordered arrays at the boundaries of the Co-T4PT networks. The corresponding fast Fourier transform (FFT) image reveals two sets of spots with identical symmetry: the inner ones (red circles) originate from the Co-T4PT networks, while the outer ones (blue circles) stem from the C₆₀ arrays. This indicates the different lattices between the two structures. The green dashed region is magnified in Figure 3c. The short-dashed lines depict the C₆₀ array following the lattice directions of the underlying network, but the molecules are not precisely located in the Co-T4PT cavities. The line profiles along the red and blue arrows show a smaller lattice of the C₆₀ array (10.5 ± 0.5 Å) than the underlying porous network (11.9 ± 0.5 Å). Remarkably, the lattice of the C₆₀ array on the Co-T4PT network is identical to that on the Co surface (line profile along the black arrow), indicating a significant interaction between the C₆₀ molecules.

Figure 3d shows two real-time STM images recorded in the purple dashed region in Figure 3b. In the left image, two isolated C₆₀ molecules are located in the Co-T4PT cavities of “1” and “2”

with a distance of 24.2 Å, almost twice the interporous distance (~ 12 Å). After a frame interval $\Delta t = 419$ s, a C_{60} molecule moves from position "2" to form a dimer with another molecule at position "3", as depicted in the image on the right. The distance in the dimer measures 10.1 Å, which is in line with the vdW diameter of C_{60} but smaller than the interporous distance. As a result, the interacting C_{60} molecules are out of the cavities. The different cases occur in the mentioned BDBA and NN4A networks, where the interporous distances are 15 Å and 26 Å, respectively, beyond the C_{60} interacting diameter. The porous potential dominates the adsorbed C_{60} molecules precisely in their cavities. The Co-T4PT network has a suitable cavity size ($D = 7.5 \pm 0.5$ Å) for the molecular confinement, but the shorter cavity distance (11.9 ± 0.5 Å) is in the range of the C_{60} interacting diameter. Therefore, the arrangement of the C_{60} molecules is steered by the competition between the Co-T4PT porous potential and the vdW interactions of the neighboring C_{60} .

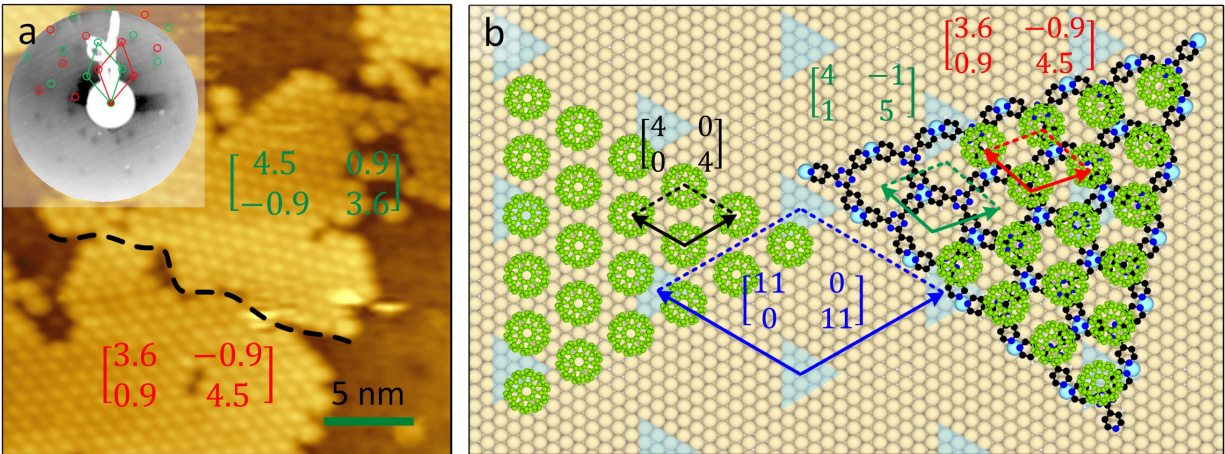


Figure 4. (a) STM topography of 0.75 ML C_{60} on 0.9 ML Co-T4PT network on 5 ML Co surface. The C_{60} domains separated by the black dashed line show the mirror structures of $\begin{bmatrix} 4.5 & 0.9 \\ -0.9 & 3.6 \end{bmatrix}$ and $\begin{bmatrix} 3.6 & -0.9 \\ 0.9 & 4.5 \end{bmatrix}$. The simulated diffraction spots (green and red circles) are superimposed on the corresponding LEED image (at 18 eV). (b) The proposed model shows the structures of C_{60} molecules adsorbed on the Co surface and on the Co-T4PT network, and the corresponding unit cells and lattice matrices are marked. The blue triangles represent the triangular dislocation loops of the Co surface. The STM was recorded at 106 K and the V_{tip} was + 0.50V in (a).

When 0.75 ML C_{60} is covered on the Co-T4PT network in Figure 4a, the molecules conform to the symmetries of the underlying networks and aggregate into the large domains. The corresponding LEED image (upper-left corner) also indicates that the C_{60} configurations have the same shape as the Co-T4PT networks (in Figure 2a), but form the smaller superlattices described by the matrices of $\begin{bmatrix} 4.5 & 0.9 \\ -0.9 & 3.6 \end{bmatrix}$ and $\begin{bmatrix} 3.6 & -0.9 \\ 0.9 & 4.5 \end{bmatrix}$. The structures of C_{60} molecules adsorbed on the Co surface and on the Co-T4PT network are illustrated in Figure 4b, with the lattice parameters

summarized in Table S1. By comparing the adsorption of C_{60} on both surfaces, the two-dimensional Co-T4PT network has been substantiated as a templating layer to tailor the ferromagnetic Co surface potential landscape.

Conclusions

The ultrathin Co films are grown on the Au(111) surface, and the lattice mismatch of the top two layers results in a well-ordered TDL reconstruction. Supported on the Co surface, the deposited T4PT molecules can coordinate with the surface Co atoms to form a large-scale Co-T4PT porous network. The Co-T4PT network contains periodic nanocavities as a quantum well array to reshape the surface potential landscape of ferromagnetic Co. Subsequently adsorbed C_{60} molecules arrange along the symmetry of the underlying porous networks, but their interactions with neighbouring molecules cause them to deviate from the cavities, resulting in a smaller lattice. Therefore, the C_{60} configurations are dominated by the Co-T4PT porous potential and the neighbouring C_{60} interactions. Our research proposes a functionalized protocol for 2D-MOPNs on ferromagnetic surfaces that can be used as templates for molecule-based electronics and spintronics.

Methods

Sample preparation. All experiments were performed in ultra-high-vacuum systems (base pressure 10^{-10} mbar) housed on an Omicron MULTIPROBE STM. Prior to deposition of adsorbates, the Au(111) surface was cleaned by several cycles of Ar-ion sputtering and subsequent annealing. The surface cleanliness was inspected using the LEED and the STM images, as shown in Figure 1a. Co evaporation was conducted by an electron beam evaporator (FOCUS EFM3) with a flux of 40 nA, and the coverage was determined by calculating a time-integrated thickness of the as-grown submonolayer in STM. The grown Co films were annealed at 560 K for 15 mins to form large-scale surface terraces¹⁷. The purified T4PT and C_{60} molecules were thermally evaporated at 450 K and 638 K, respectively, while the samples were at room temperature. The molecular deposition rates were 0.25 ML/min for T4PT and 0.06 ML/min for C_{60} monitored by a quartz crystal microbalance (QCM), and the coverage was calibrated by the STM. The T4PT molecules deposited on the 5 ML Co were annealed at 413 K for 60 mins to fabricate the Co-T4PT network. The grown C_{60} films were not further annealed in the experiments.

Scanning tunneling microscopy (STM). The STM setup has been reported in previous work³⁴. In brief, all STM topographies were recorded in constant current mode with a tunneling current (I_t) in the range of 70-90 pA. The bias voltage (V_{tip}) was applied to the STM tip, where positive and negative values corresponded to the occupied and unoccupied states of the samples, respectively. The low-temperature STM experiments at 106 K were conducted using a liquid N_2 system. The STM data were processed using the WSxM and the Gwyddion softwares^{35,36}.

Low energy electron diffraction (LEED). The LEED images were obtained using a rear view four grid system at room temperature, and some diffraction spots were overlaid with the corresponding matrices simulated in Spot-Plotter Software³⁷.

References

1. Barth, J. V. Fresh perspectives for surface coordination chemistry. *Surf Sci* **603**, 1533-1541 (2009).
2. Gutzler, R., Stepanow, S., Grumelli, D., Lingenfelder, M., Kern, K. Mimicking enzymatic active sites on surfaces for energy conversion chemistry. *Acc Chem Res* **48**, 2132-2139 (2015).
3. Abdurakhmanova, N. et al. Superexchange-mediated ferromagnetic coupling in two-dimensional Ni-TCNQ networks on metal surfaces. *Phys Rev Lett* **110**, 027202 (2013).
4. Giovanelli, L. et al. Magnetic Coupling and Single-Ion Anisotropy in Surface-Supported Mn-Based Metal-Organic Networks. *Journal of Physical Chemistry C* **118**, 11738-11744 (2014).
5. Muller, K., Enache, M., Stohr, M. Confinement properties of 2D porous molecular networks on metal surfaces. *J Phys Condens Matter* **28**, 153003 (2016).
6. Dong, L., Gao, Z. A., Lin, N. Self-assembly of metal-organic coordination structures on surfaces. *Progress in Surface Science* **91**, 101-135 (2016).
7. Li, J. et al. Low-Dimensional Metal-Organic Coordination Structures on Graphene. *Journal of Physical Chemistry C* **123**, 12730-12735 (2019).
8. Crommie, M. F., Lutz, C. P., Eigler, D. M. Confinement of electrons to quantum corrals on a metal surface. *Science* **262**, 218-220 (1993).
9. Lobo-Checa, J. et al. Band formation from coupled quantum dots formed by a nanoporous network on a copper surface. *Science* **325**, 300-303 (2009).
10. Nowakowska, S. et al. Configuring Electronic States in an Atomically Precise Array of Quantum Boxes. *Small* **12**, 3757-3763 (2016).
11. Stöhr, M., Wahl, M., Spillmann, H., Gade, L. H., Jung, T. A. Lateral manipulation for the positioning of molecular guests within the confinements of a highly stable self-assembled organic surface network. *Small* **3**, 1336-1340 (2007).
12. Sun, M. F., Mi, W. B. Progress in organic molecular/ferromagnet spinterfaces: towards molecular spintronics. *Journal of Materials Chemistry C* **6**, 6619-6636 (2018).
13. Mittendorfer, F., Hafner, J. initial steps in the desulfurization of thiophene/Ni(100) - A DFT study. *Journal of Catalysis* **214**, 234-241 (2003).
14. Vu, A. D., Coraux, J., Chen, G., N'Diaye, A. T., Schmid, A. K., Rougemaille, N. Unconventional magnetisation texture in graphene/cobalt hybrids. *Sci Rep* **6**, 24783 (2016).
15. Auwärter, W. Hexagonal boron nitride monolayers on metal supports: Versatile templates for atoms, molecules and nanostructures. *Surface Science Reports* **74**, 1-95 (2019).
16. Barth, J. V., Brune, H., Ertl, G., Behm, R. J. Scanning tunneling microscopy observations on the reconstructed Au(111) surface: Atomic structure, long-range superstructure, rotational domains, and surface defects. *Physical Review B* **42**, 9307-9318 (1990).
17. Haag, N. et al. Epitaxial growth of thermally stable cobalt films on Au(111). *New Journal of Physics* **18**, (2016).
18. Kollamana, J. et al. Scanning Tunneling Microscopy Study of Ordered C60 Submonolayer Films on Co/Au(111). *The Journal of Physical Chemistry C* **120**, 7568-7574 (2016).
19. Pochet, P., McGuigan, B. C., Coraux, J., Johnson, H. T. Toward Moiré engineering in 2D materials via dislocation theory. *Applied Materials Today* **9**, 240-250 (2017).
20. Jacobsen, J. et al. Atomic-scale determination of misfit dislocation loops at metal-metal interfaces. *Phys Rev Lett* **75**, 489-492 (1995).
21. Meunier, I., Trégliat, G., Gay, J.-M., Aufray, B., Legrand, B. Ag/Cu(111) structure revisited through an extended mechanism for stress relaxation. *Physical Review B* **59**, 10910-10917 (1999).
22. Bendounan, A., Cercellier, H., Fagot-Revurat, Y., Kierren, B., Yurov, V. Y., Malterre, D. Modification of Shockley states induced by surface reconstruction in epitaxial Ag films on Cu(111). *Physical Review B* **67**, 165412 (2003).

23. Umbach, T. R. et al. Ferromagnetic coupling of mononuclear Fe centers in a self-assembled metal-organic network on Au(111). *Phys Rev Lett* **109**, 267207 (2012).
24. Umbach, T. R. et al. Site-specific bonding of copper adatoms to pyridine end groups mediating the formation of two-dimensional coordination networks on metal surfaces. *Physical Review B* **89**, 235409 (2014).
25. Classen, T. et al. Templated growth of metal–organic coordination chains at surfaces. *Angewandte Chemie-International Edition* **44**, 6142-6145 (2005).
26. Piquero-Zulaica, I. et al. Engineering quantum states and electronic landscapes through surface molecular nanoarchitectures. *Rev Mod Phys* **94**, 045008 (2022).
27. Plas, J., Ivashenko, O., Martsinovich, N., Lackinger, M., De Feyter, S. Nanopatterning of a covalent organic framework host–guest system. *Chemical Communications* **52**, 68-71 (2016).
28. Li, M. et al. Site - selective fabrication of two - dimensional fullerene arrays by using a supramolecular template at the liquid - solid interface. *Angewandte Chemie-International Edition* **47**, 6717-6721 (2008).
29. Haag, N. et al. Signatures of an atomic crystal in the band structure of a C₆₀ thin film. *Physical Review B* **101**, 165422 (2020).
30. Reddy, C. D., Yu, Z. G., Zhang, Y.-W. Two-dimensional van der Waals C₆₀ molecular crystal. *Scientific Reports* **5**, 12221 (2015).
31. Jung, M., Shin, D., Sohn, S.-D., Kwon, S.-Y., Park, N., Shin, H.-J. Atomically resolved orientational ordering of C₆₀ molecules on epitaxial graphene on Cu(111). *Nanoscale* **6**, 11835-11840 (2014).
32. Kiguchi, M., Iizumi, K.-i., Saiki, K., Koma, A. Atomic and electronic structures of heteroepitaxial C₆₀ film grown on Ni(1 1 1), Cu(1 1 1). *Applied Surface Science* **212-213**, 101-104 (2003).
33. Altman, E. I., Colton, R. J. Determination of the orientation of C₆₀ adsorbed on Au(111) and Ag(111). *Phys Rev B* **48**, 18244-18249 (1993).
34. Lyu, L. et al. Thermal-Driven Formation of 2D Nanoporous Networks on Metal Surfaces. *Journal of Physical Chemistry C* **123**, 26263-26271 (2019).
35. Horcas, I., Fernandez, R., Gomez-Rodriguez, J. M., Colchero, J., Gomez-Herrero, J., Baro, A. M. WSXM: A software for scanning probe microscopy and a tool for nanotechnology. *Rev Sci Instrum* **78**, 013705 (2007).
36. Nečas, D., Klapetek, P. Gwyddion: an open-source software for SPM data analysis. *Open Physics* **10**, 181-188 (2012).
37. Bayersdorfer, P. <http://spot-plotter.software.informer.com>.

Acknowledgments

This work was supported by the Deutsche Forschungsgemeinschaft (DFG, German Research Foundation), TRR 173-268565370 Spin + X: spin in its collective environment (Project B05). B.S. acknowledges financial support by the Dynamics and Topology Center funded by the State of Rhineland Palatinate.

Tailoring the ferromagnetic surface potential landscape by a templating two-dimensional metal-organic network

by
L. Lyu et al.

Supplementary Figures

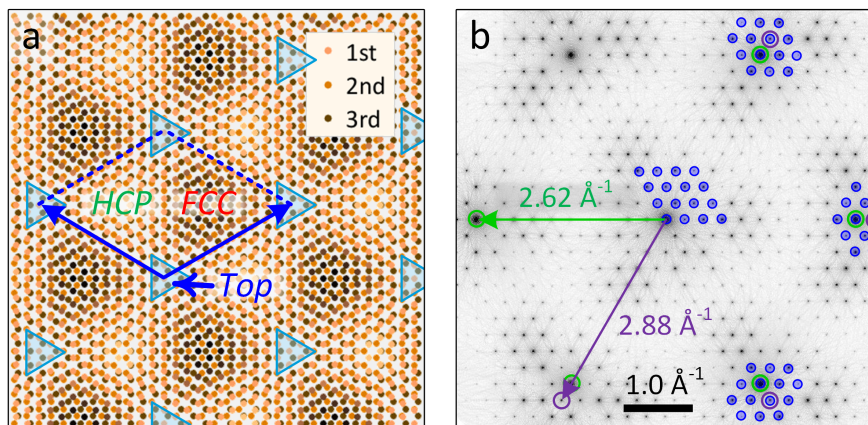


Figure S1. (a) The model of the top three layers Co for the LEED simulation. The Co atoms have the same symmetry in each layer, but the $d_{\text{Co-Co}}$ lattices are 2.52 Å in the 1st layer and 2.77 Å in the 2nd and 3rd layers. The three types of atom stacking faults are found in the surface regions: HCP (A-B-A), FCC (A-B-C) and Top (A-A-A). The blue triangles mark the top stacking regions, forming a (11 × 11) lattice (the blue rhombus). (b) The simulated diffraction structures, including the reciprocal lattices of the 1st layer Co (purple circles, $\frac{2\pi}{2.52} \times \frac{2}{\sqrt{3}} = 2.88 \text{ \AA}^{-1}$), the 2nd layer Co (green circles, $\frac{2\pi}{2.77} \times \frac{2}{\sqrt{3}} = 2.62 \text{ \AA}^{-1}$) and the atom stacking faults (blue circles, 11 × 11). The diffraction simulation was performed in the Matlab program[S1].

[S1] Martocchia, D. et al. Graphene on Ru(0001): a corrugated and chiral structure. *New Journal of Physics* **12**, 043028 (2010).

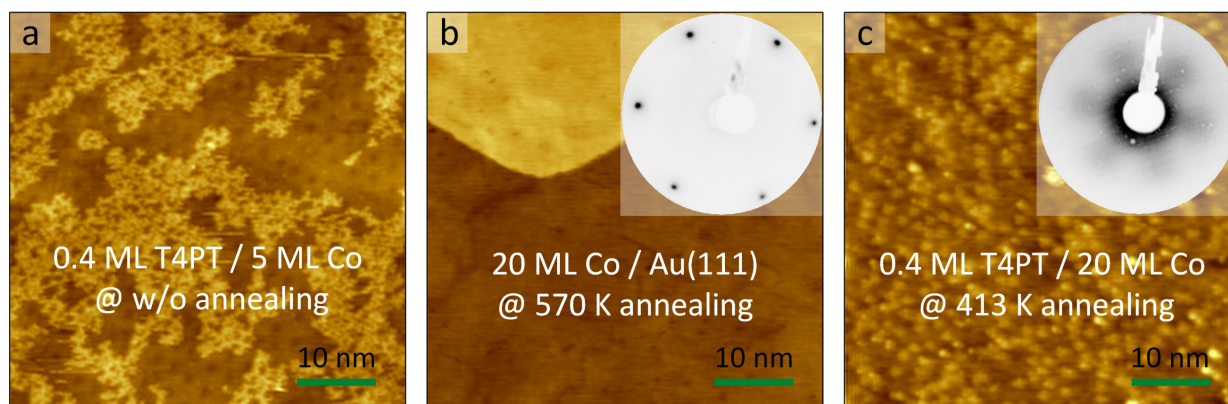


Figure S2. (a) STM topography of 0.4 ML T4PT on 5 ML Co surface prior to the annealing process (w/o annealing). (b) STM topography of 20 ML Co on Au(111) after annealing of 570 K, and the upper-left LEED image (at 60 eV) indicates the bulk-phase Co structure. (c) STM topography of 0.4 ML T4PT on 20 ML Co surface after annealing of 413 K. The T4PT molecules are disordered on the surface, and the corresponding LEED image (at 12 eV) shows the blurred spots. All STM images were recorded at 106 K, and the V_{tip} was + 0.71 V in (a), + 0.29 V in (b) and + 0.95 V in (c).

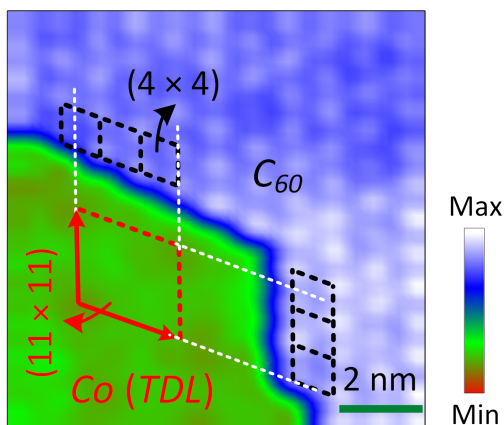


Figure S3. STM image of 0.6 ML C_{60} on 5 ML Co surface. The red rhombus is the unit cell of the Co TDL structure (11×11), which extends the lattice (white dashed lines) to the adsorbed C_{60} unit cells (black rhombi, 4×4). The STM was acquired at 106 K, and the V_{tip} was -0.08 V.

Table S1. Summary of the structural parameters (unit cell and lattice matrix) for 5 ML Co / Au(111), C_{60} / 5 ML Co, Co-T4PT / 5 ML Co, and C_{60} / Co-T4PT / 5 ML Co. The lattice matrices are obtained by fitting the LEED spots. Each unit cell is calibrated by the corresponding matrix, excluding reasonable errors. γ is the angle of the lattice vectors $\langle \mathbf{a}, \mathbf{b} \rangle$ and $\langle \mathbf{A}, \mathbf{B} \rangle$. The basis vectors for all the matrices are $|\mathbf{a}| = |\mathbf{b}| = 2.52 \text{ \AA}$ and $\gamma = 120^\circ$.

Geometry	Unit Cell	Matrix
5 ML Co / Au(111)	$ \mathbf{a} = \mathbf{b} = 2.52 \text{ \AA}, \gamma = 120^\circ$	$\begin{bmatrix} 11 & 0 \\ 0 & 11 \end{bmatrix} (\text{TDL})$
	$ \mathbf{A} = \mathbf{B} = 27.72 \text{ \AA}, \gamma = 120^\circ (\text{TDL})$	
$\text{C}_{60} / 5 \text{ ML Co} / \text{Au}(111)$	$ \mathbf{A} = \mathbf{B} = 10.08 \text{ \AA}, \gamma = 120^\circ$	$\begin{bmatrix} 4 & 0 \\ 0 & 4 \end{bmatrix}$
Co-T4PT / 5 ML Co / Au(111)	$ \mathbf{A} = \mathbf{B} = 11.55 \text{ \AA}, \gamma = 120^\circ$	$\begin{bmatrix} 5 & 1 \\ -1 & 4 \end{bmatrix} / \begin{bmatrix} 4 & -1 \\ 1 & 5 \end{bmatrix}$
$\text{C}_{60} / \text{Co-T4PT} / 5 \text{ ML Co} / \text{Au}(111)$	$ \mathbf{A} = \mathbf{B} = 10.39 \text{ \AA}, \gamma = 120^\circ$	$\begin{bmatrix} 4.5 & 0.9 \\ -0.9 & 3.6 \end{bmatrix} / \begin{bmatrix} 3.6 & -0.9 \\ 0.9 & 4.5 \end{bmatrix}$